Journal of Process Control 32 (2015) 98–108

Contents lists available at ScienceDirect

Journal of Process Control

journal homepage: www.elsevier.com/locate/jprocont

Handling state constraints and economics in feedback control of transport-reaction processes

Liangfeng Lao[a], Matthew Ellis[a], Panagiotis D. Christofides[a,b,*]

[a] Department of Chemical and Biomolecular Engineering, University of California, Los Angeles, CA 90095, USA
[b] Department of Electrical Engineering, University of California, Los Angeles, CA 90095, USA

ARTICLE INFO

Article history:
Received 14 April 2014
Received in revised form 18 February 2015
Accepted 13 April 2015
Available online 8 May 2015

Keywords:
Economic model predictive control
Parabolic partial differential equations
Transport-reaction processes

ABSTRACT

Transport-reaction processes, which are typically described by parabolic partial differential equations (PDEs), play an important role within the chemical process industries. Therefore, it is important to develop feedback control techniques that operate transport-reaction processes in an economically optimal fashion in the presence of constraints in the process states and manipulated inputs. Economic model predictive control (EMPC) is a predictive control scheme that combines process economics and feedback control into an integrated framework with the potential of improving the closed-loop process economic performance compared to traditional control methodologies. In this work, we focus on systems of nonlinear parabolic PDEs and propose a novel EMPC design integrating adaptive proper orthogonal decomposition (APOD) method with a high-order finite-difference method to handle state constraints. The computational efficiency and constraint handling properties of this design are evaluated using a tubular reactor example modeled by two nonlinear parabolic PDEs.

1. Introduction

The development of computationally efficient control methods for partial differential equation (PDE) systems has been a major research topic in the past 30 years (e.g., [6]). The design of feedback control algorithms for PDE systems is usually achieved on the basis of finite-dimensional systems (i.e., sets of ordinary differential equations (ODEs) in time) obtained by applying a variety of spatial discretization and/or order reduction methods to the PDE system. The classification of PDE systems, which is based on the properties of the spatial differential operator into hyperbolic, parabolic, or elliptic, typically determines the finite-dimensional approximation approaches employed to derive finite-dimensional models (e.g., [6,24]). A class of processes described by PDEs within chemical process industries is transport-reaction processes. For example, tubular reactors are typically described by parabolic PDEs since both convective and diffusive transport phenomena are significant.

For parabolic PDE systems (e.g., diffusion-convective-reaction processes) whose dominant dynamics can be adequately represented by a finite number of dominant modes, Galerkin's method with spatially global basis functions is a good way among many weighted residual methods (e.g., [9,21]) to construct a reduced-order model (ROM) of the PDE system. Specifically, it can be used to derive a finite-dimensional ODE model by applying approximate inertial manifolds (AIMs) (e.g., [10]) that capture the dominant dynamics of the original PDE system. The basis functions used in Galerkin's method may either be analytical or empirical eigenfunctions. After applying Galerkin's method to the PDE system and a low-order ODE system is derived, the control system can be designed by utilizing control methods for linear/nonlinear ODE systems [6].

One way to construct the empirical eigenfunctions is by applying proper orthogonal decomposition (POD) (e.g., [23,12,15]) to PDE solution data. This data-based methodology for constructing the basis eigenfunctions has been widely adopted in the field of model-based control of parabolic PDE systems (e.g., [5,25,4,17,15]). However, to achieve high accuracy of the ROM derived from the empirical eigenfunctions of the original PDE system, the POD method usually needs a large ensemble of solution data (snapshots) to contain as much local and global process dynamics as possible. Constructing such a large ensemble of snapshots becomes a significant challenge from a practical point of view; because currently, there is no general way to realize a representative ensemble. Based on this consideration, an adaptive proper orthogonal decomposition (APOD) methodology was proposed to recursively update the ensemble of snapshots and compute on-line the new empirical

* Corresponding author at: Department of Chemical and Biomolecular Engineering, University of California, Los Angeles, CA 90095, USA. Tel.: +1 310 794 1015; fax: +1 310 206 4107.
E-mail address: pdc@seas.ucla.edu (P.D. Christofides).

http://dx.doi.org/10.1016/j.jprocont.2015.04.009
0959-1524/

eigenfunctions in the on-line closed-loop operation of PDE systems (e.g., [20,22,26,19]). While the APOD methodology of [26,19] demonstrated its ability to capture the dominant process dynamics by a relatively small number of snapshots which reduces the overall computational burden, these works did not address the issue of computational efficiency with respect to optimal control action calculation and input and state constraint handling. Moreover, the ROM accuracy is limited by the number of the empirical eigenfunctions adopted for the ROM; in practice, when a process faces state constraints, the accuracy of the ROM based on a limited number of eigenfunctions may not be able to allow the controller to avoid a state constraint violation.

Economic model predictive control (EMPC) is a practical optimal control-based technique that has recently gained widespread popularity within the process control community and beyond because of its unique quality of effectively integrating process economics and feedback control (see [8] for an overview of recent results and references). It deals with a reformulation of the conventional MPC quadratic cost function in which an economic (not necessarily quadratic) cost function is used directly as the cost in MPC, and, it may, in general, lead to time-varying process operation policies (instead of steady-state operation), which directly optimize process economics. However, most of previous EMPC systems have been designed for lumped parameter processes described by linear/nonlinear ODE systems (e.g., [1,2,14,11,13]). In our previous work ([16,15]), an EMPC system with a general economic cost function for parabolic PDE systems was proposed which operates the closed-loop system in a dynamically optimal fashion. Specifically, the EMPC scheme was developed on the basis of low-order nonlinear ODE models derived through Galerkin's method using analytical eigenfunctions [16] and empirical eigenfunctions derived by POD [15], respectively. However, no work has been done on applying APOD techniques for model order reduction to parabolic PDE systems under EMPC. Typically, EMPC will operate a system at its constraints in order to achieve the maximum closed-loop economic performance benefit. Thus, the challenge is to formulate EMPC schemes that can handle state constraints (i.e., prevent state constraint violation).

Motivated by the above considerations, in this work, we apply APOD to parabolic PDE systems by considering process control system computational efficiency and some specific constraints imposed on the process (i.e., state and input constraints), and propose a novel EMPC design integrating APOD method with a high-order finite-difference method. The proposed EMPC method is applied to a non-isothermal tubular reactor where a second-order chemical reaction takes place and the computational efficiency, state and input constraint satisfaction, and closed-loop economic performance are evaluated.

2. Preliminaries

2.1. Parabolic PDEs

We consider parabolic PDEs of the form:

$$\frac{\partial x}{\partial t} = A\frac{\partial x}{\partial z} + B\frac{\partial^2 x}{\partial z^2} + Wu(t) + f(x) \tag{1}$$

with the boundary conditions:

$$\frac{\partial x}{\partial z}|_{z=0} = g_0 x(0,t), \quad \frac{\partial x}{\partial z}|_{z=1} = g_1 x(1,t) \tag{2}$$

for $t \in [0, \infty)$ and the initial condition:

$$x(z,0) = x_0(z) \tag{3}$$

where $z \in [0, 1]$ is the spatial coordinate, $t \in [0, \infty)$ is the time, $x(z,t) = [x_1(z,t) \dots x_{n_x}(z,t)]^T \in \mathbb{R}^{n_x}$ is the vector of the state variables (x^T denotes the transpose of x), and $f(x)$ denotes a nonlinear vector function. The notation A, B, W, g_0 and g_1 is used to denote (constant) matrices of appropriate dimensions. The control input vector is denoted as $u(t) \in \mathbb{R}^{n_u}$ and is subject to the following constraints:

$$u_{\min} \le u(t) \le u_{\max} \tag{4}$$

where u_{min} and u_{max} are the lower and upper bound vectors of the manipulated input vector, $u(t)$. Moreover, the system states are also subject to the following state constraints:

$$x_{i,\min} \le \int_0^1 r_{x_i}(z) x_i(z,t) dz \le x_{i,\max} \tag{5}$$

for $i = 1, \dots, n_x$ where $x_{i,min}$ and $x_{i,max}$ are the lower and upper state constraint for the i-th state, respectively. The function $r_{x_i}(z) \in L_2(0,1)$ where $L_2(0,1)$ is the space of measurable square-integrable functions on the interval [0, 1], is the state constraint distribution function.

2.2. Galerkin's method with POD-computed basis functions

To reduce the PDE model of Eq. (1) into an ODE model, we take advantage of the orthogonality of the empirical eigenfunctions obtained from POD ([23,12]). Specifically, using Galerkin's method ([7,10]), a low-order ODE system for the PDEs of Eq. (1) describing the temporal evolution of the amplitudes corresponding to the first m_i eigenfunctions of the i-th PDE state in Eq. (1) has the following form:

$$\begin{aligned} &\dot{a}_s(t) = \mathcal{A}_s a_s(t) + \mathcal{F}_s(a_s(t)) + \mathcal{W}_s u(t) \\ &x_i(z,t) \approx \sum_{j=1}^{m_i} a_s^{ij}(t)\phi_{ij}(z), \quad i = 1, \dots, n_x \end{aligned} \tag{6}$$

where $a_s(t) = [a_{s,1}^T(t) \dots a_{s,n_x}^T(t)]^T$ is a vector of the total eigenmodes, $a_{s,i}(t) = [a_s^{i1}(t) \dots a_s^{im_i}(t)]^T$ is a vector of the amplitudes of the first m_i eigenfunctions, $a_s^{ij}(t)$ is the $j-th$ eigenmode of $i-th$ PDE, $\mathcal{A}_s$ and $\mathcal{W}_s$ are constant matrices, $\mathcal{F}_s(a_s(t))$ is a nonlinear smooth vector function of the modes obtained by applying weighted residual method to Eq. (1), and $\{\phi_{ij}(z)\}_{j=1:m_i}$ are the first m_i dominant empirical eigenfunctions computed from POD for the i-th PDE state, $x_i(z,t)$.

3. EMPC of parabolic PDE systems with state and control constraints

3.1. Adaptive proper orthogonal decomposition

Compared with POD, APOD is a more computationally efficient algorithm because it only needs an ensemble of a small number of snapshots in the beginning. It can complete the recursive update of the computation of the dominant eigenfunctions, while keeping the size of the ensemble small to reduce the computational burden of updating the ensemble once a new process state measurement is available. Moreover, APOD can also adaptively adjust the number of the basis eigenfunctions under a desired energy occupation requirement, η. Out of N possible eigenvalues from the covariance matrix of the ensemble, the most dominant m eigenvalues of the covariance matrix occupies η energy of the whole ensemble, i.e., $\sum_{j=1}^{m}\lambda_j / \sum_{j=1}^{N}\lambda_j \le \eta$. Then, the computational efficiency of the control system whose construction is based on the ROM with the dominant eigenfunctions will be improved due to the adaptive property of APOD [26]. Since the basis eigenfunctions are

updated on-line, the initial ensemble of process snapshots may contain significantly less process solution data than POD. More details of the APOD methodology can be found in [26] and [19]. The implementation steps of the APOD methodology can be summarized as follows:

1. At $t<0$, generate an ensemble of solutions of the PDE system (e.g., Eq. (1)) for single manipulated input value $u(t)$ from certain initial condition;
   1.1. Apply POD to this ensemble to derive a set of first $m_i(t_0)$ most dominant empirical eigenfunctions for each state x_i, $i=1,\ldots,n_x$ which occupy η energy of the chosen ensemble [3];
   1.2. Construct a ROM in the form of a low-dimensional nonlinear ODE system based on these empirical eigenfunctions within a Galerkin's model reduction framework from the infinite dimensional nonlinear PDE system;
2. The ensemble (or basis eigenfunctions) is updated based on a constant update frequency with the update period, Δ (constant). In the context of EMPC, the update period, Δ, is equal to the sampling time in EMPC. For all k, repeat: at $t=t_k=k\Delta>0$, when the new process state measurements are available, update the ensemble by utilizing the most important snapshots approach [19] which analyzes the contribution of the current snapshots in the ensemble and replaces the snapshot that corresponds to the lowest contribution of representativeness with new state measurement to keep the size of the ensemble the same;
   2.1. Recompute the dominant eigenvalues corresponding to the first $m_i(t_{k-1})$ eigenfunctions by constructing small scale matrix to reduce the computational burden;
   2.2. Adopt orthogonal power iteration methodology to get the $(m_i(t_{k-1})+1)-th$ dominant eigenvalue;
   2.3. Get the new size of the basis eigenfunctions, $m_i(t_k)$ which should still occupy η energy of the updated ensemble (the new size of the basis eigenfunctions, $m_i(t_k)$, may increase, decrease or keep the same compared with $m_i(t_{k-1})$);

3.2. Methodological framework for finite-dimensional EMPC using adaptive proper orthogonal decomposition

3.2.1. EMPC using adaptive POD

Utilizing the empirical eigenfunctions from APOD, we formulate a state feedback Lyapunov-based EMPC for the system of Eq. (1) to dynamically optimize an economic cost function. We assume that the state profile across the entire spatial domain is available synchronously at sampling instants denoted as $t_k=k\Delta$ with $k=0,1,\ldots$. To formulate a finite-dimensional EMPC problem, the first m_i modes of Eq. (6) are adopted to construct the ROM, and the EMPC formulation takes the following form:

$$\max_{u\in S(\Delta)} \int_{t_k}^{t_{k+N}} L_e(\tau)d\tau \tag{7a}$$

$$\text{s.t.} \quad \dot{a}_s(t)=\mathcal{A}_s a_s(t)+\mathcal{F}_s(a_s(t))+\mathcal{W}_s u(t), \tag{7b}$$

$$a_s^{ij}(t_k)=\int_0^1 \phi_{ij}(z)x_i(z,t_k)dz, \quad \text{for } j=1,\ldots,m_i \tag{7c}$$

$$\hat{x}_i(z,t)=\sum_{j=1}^{m_i} a_s^{ij}(t)\phi_{ij}(z), \tag{7d}$$

$$u_{\min}\le u(t)\le u_{\max}, \tag{7e}$$

$$x_{i,\min}\le \int_0^1 r_{x_i}(z)\hat{x}_i(z,t)dz\le x_{i,\max}, \tag{7f}$$

$$a_s^T(t)Pa_s(t)\le \overline{\rho} \tag{7g}$$

where the constraints are enforced for all $t\in[t_k, t_{k+N})$ and $i=1,\ldots,n_x$, Δ is the sampling period, $S(\Delta)$ is the family of piecewise constant functions with sampling period Δ, N is the prediction horizon, $\hat{x}_i(z,t)$ is the predicted evolution of state variables with input $u(t)$ computed by the EMPC and $x_i(z,t_k)$ is the state measurement at the sampling time t_k. Since the empirical eigenfunctions derived from the APOD procedure are all self-adjoint, i.e., $\{\overline{\phi}_{ij}(z)\}=\{\phi_{ij}(z)\}$ (more details can be found in [23,12]), we can use the empirical eigenfunction $\{\phi_{ij}(z)\}$ directly to calculate the estimated eigenmode amplitude $a_s^{ij}(t_k)$ by taking advantage of the orthogonality property of the eigenfunctions in Eq. (7c).

In the optimization problem of Eq. (7), the objective function of Eq. (7a) describes the temporal economic cost of the process which the EMPC maximizes over a horizon $N\Delta$. The constraint of Eq. (7b) is used to predict the future evolution of the subsystem based on the first m_i dominant eigenfunctions with the initial condition given in Eq. (7c) (i.e., the estimate of $a_s^{ij}(t_k)$ computed from the state measurement $x_i(z,t_k)$). The constraints of Eq. (7e)–(7f) are the available control action and the state constraints, respectively. Finally, the constraint of Eq. (7g) ensures that the predicted state trajectory is restricted inside a predefined stability region, $\overline{\rho}$ which is a level set of a quadratic Lyapunov function $V(a_s)=a_s^TPa_s$ where P is a positive definite matrix (see [11] for a complete discussion of this issue). The optimal solution to this optimization problem is $u^*(t|t_k)$ defined for $t\in[t_k, t_{k+N})$. The EMPC applies the control action computed for the first sampling period to the system in a sample-and-hold fashion for $t\in[t_k, t_{k+1})$. The EMPC is resolved at each sampling period, t_{k+1}, after receiving a new state measurement of each state, $x_i(z,t_{k+1})$ and updating basis functions, $\{\phi_{ij}(z)\}$ from APOD.

3.2.2. EMPC scheme of integrating APOD and finite-difference method to avoid state constraint violation and improve computational efficiency

Although APOD only needs an ensemble of a small number of snapshots which can improve the computational efficiency of the eigenfunction update calculation, smaller size of ensemble usually results in a single or a few dominant eigenfunctions. The accuracy of the ROM based on fewer eigenfunctions computed from an ensemble of small size is usually worse than that of the ROM constructed by adopting more eigenfunctions from a large ensemble of snapshots. However, as pointed out in [18], eigenfunctions that have high frequency spatial profiles (corresponding to small empirical eigenvalues) should be discarded because of potentially significant round-off errors. In this situation, only a single or a few eigenfunctions can be adopted from APOD keeping the dimension of the reduced-order model low. So there exists a trade-off between the ROM accuracy and computational efficiency of APOD in practical implementation. Moreover, under a dynamic operation of a process, the state error between the estimated state value from ROM and the actual state value cannot be predicted (i.e., it is almost impossible to predict whether the estimated state value will be an overestimate or an underestimate of the actual state value). From the point of view of practical implementation, when the process faces some specific state constraints, a controller which is constructed based on the ROM may produce an input trajectory misleading the process to violate state constraints.

To circumvent this problem, we propose an EMPC methodology to avoid potential state constraint violation. The methodology integrating APOD and a high-order finite-difference method in EMPC is designed to improve the computational efficiency compared to using EMPC with a model constructed from a high-order finite-difference method only. Before a detailed algorithm of the methodology can be presented, we define the following notation which will be used in the algorithm. To ensure that the state

constraint is satisfied, we will make use of the following two inequalities to define a so-called alert region:

$$\int_0^1 r_{x,i}(z)x_i(z,t)dz \geq x_{i,\max}^{alert}, \tag{8a}$$

$$\int_0^1 r_{x,i}(z)x_i(z,t)dz \leq x_{i,\min}^{alert} \tag{8b}$$

where $x_{i,\max}^{alert} < x_{i,\max}$ and $x_{i,\min}^{alert} > x_{i,\min}$ are tuning parameters chosen to ensure that the state constraints are always satisfied under the EMPC methodology described below. With abuse of notation, we use $x_i(z,t) \in \Omega_i$ to denote the fact that one of the inequalities of Eq. (8) is satisfied for the state profile of the i-th PDE state, and we use $x_i(z,t) \notin \Omega_i$ to denote that neither inequalities are satisfied. Also, Ω_i is referred to as the i-th state constraint alert region. The abbreviation EMPC-FD will denote an EMPC scheme formulated with a model from a high-order finite-difference method, while EMPC-APOD will be used to denote an EMPC with a model resulting from APOD. The corresponding input trajectory from each EMPC will be denoted as $u_{FD}(t|t_k)$ and $u_{APOD}(t|t_k)$, respectively. The algorithm is initialized with POD, that is an ensemble of solutions of the PDE system of Eq. (1) are collected, m_i is derived by applying standard POD method to the initial ensemble for each state, and an EMPC with a model generated through POD computes the control action for the first sampling period (i.e., from $t=0$ to $t=\Delta$). The control action applied to the system over the first sampling period is denoted as $u^*(t_0) = u_{POD}(t|t_0)$ and $k=0$.

Considering that the APOD procedure (i.e., updating the empirical eigenfunctions) is computationally expensive especially when the size of the ensemble is large, the state measurement value $x(z, t_k)$ is adopted to update the basis eigenfunctions by APOD procedure for ROM construction at $t=t_{k+1}$ which is completed during the sampling time between $t=t_k$ and $t=t_{k+1}$. In other words, the APOD update is performed over the sampling period t_k to t_{k+1} in parallel to the EMPC calculation that is done at a sampling instance t_k. The detailed steps of EMPC system flow chart which integrates the APOD methodology with a finite-difference method are explained as follows:

Basis update procedure

1. At t_k, obtain a measurement of the state profile, go to Step 2.
2. Use the state profile measurement $x(z, t_k)$ to complete the APOD procedure and compute the number of the basis eigenfunctions for the next sampling period, $m(t_{k+1})$ where $m(t_{k+1}) = [m_1(t_{k+1}) \dots m_{n_x}(t_{k+1})]^T$ is a vector containing the number of basis eigenfunctions for each PDE state; go to Step 3.
3. If $u^*(t_k) = u_{FD}(t_k)$, go to Step 4; otherwise, go to Step 5.
4. Enforce the number of the basis eigenfunctions to be increased by 1 for the i-th PDE state (each): $m_i(t_{k+1}) = m_i(t_{k+1}) + 1$ (increase the ROM accuracy by using more eigenfunctions since the process enters into the state constraint alert region) and update the basis eigenfunctions for the i-th PDE state; go to Step 5.
5. $k \leftarrow k+1$; go to Step 1.

EMPC computational procedure

1. Obtain a measurement of the state profile at t_k; go to Step 2.
2. Solve the EMPC-APOD problem using the updated basis eigenfunctions with the size of $m(t_k)$ and get the trial input trajectory, $u_{APOD}(t|t_k)$; go to Step 3.
3. If $x_i(z, t_k) \in \Omega_i$, go to Step 3.1. Else, set the actual optimal input trajectory, $u^*(t_k) = u_{APOD}(t_k|t_k)$; go to Step 4.
   3.1. Apply the trial optimal input trajectory u_{APOD} to the finite-difference model and compute the predicted state at the next sampling time instant, $\hat{x}(z, t_{k+1})$. If $\hat{x}_i(z, t_{k+1})$ violates the state constraints, go to Step 3.2. Else, $u^*(t_k) = u_{APOD}(t_k|t_k)$ and go to Step 4.
   3.2 Solve the EMPC-FD problem to compute new trial input trajectory, $u_{FD}(t|t_k)$, and set $u^*(t_k) = u_{FD}(t_k|t_k)$; go to Step 4.
4. Apply the optimal control action $u^*(t_k)$ over the sampling period from $t=t_k$ to $t=t_{k+1}$ and $k \leftarrow k+1$; go to Step 1.

Fig. 1 illustrates the designed EMPC system flow chart for increasing the computational efficiency and avoiding potential state constraint violation. With respect to the APOD update cycle length, the availability of the full state profile across the entire spatial domain is assumed at each sampling instance (i.e., $t=t_k=k\Delta$) and the update cycle of APOD is equal to the sampling time of EMPC, Δ. Based on the proposed methodology, the computational time of APOD procedure (Steps 2 and 3 noted as "Basis Update Procedure" in Fig. 1) is not accounted for in the total EMPC calculation time (Steps 3.1 and 3.2 noted as "EMPC Computational Procedure" in Fig. 1).

Remark 1. We note here that in practice, the sampling time length Δ should be longer than the time needed to complete the APOD procedure otherwise the EMPC system will not be able to get the updated basis eigenfunctions at the new sampling time instant $t=t_{k+1}$. On the other hand, since the state measurements are available only at every Δ, large Δ may result in APOD missing the appearance of new process dynamics when the process goes through different regions in the state-space. Based on this consideration, the sampling should be chosen properly.

Remark 2. By setting the state constraint alert region of state constraint, the EMPC based on the ROM from APOD or POD method with few modes may lead to state constraint violation. However, the EMPC system based on a high-order discretization of the PDE system by finite-difference method can provide more accurate optimal manipulated input values to avoid potential state constraint violation.

Remark 3. In terms of the effectiveness of eigenfunctions, eigenfunctions that have high frequency spatial profiles (i.e., corresponding to small eigenvalues) should be discarded because of potentially significant round-off errors. When implementing the proposed methodology, the eigenfunctions corresponding to eigenvalues smaller than λ_{min} are not included to avoid round-off errors. This consideration is implemented in Steps 1 and 2.1 of Fig. 1. Furthermore, one may set the maximum number of basis functions used in APOD to avoid using eigenfunctions with high frequency spatial profiles.

Remark 4. Since the energy occupation percentage η has no direct relationship with the state prediction accuracy, to ensure the state constraint satisfaction during the whole process operation, the state violation alert region Ω_i should be large enough for a specific energy occupation requirement. For the process state outside the chosen state violation alert region Ω_i, the EMPC using APOD only is assumed to not lead the process to violate the state constraint under its ROM's accuracy.

4. Application to a tubular reactor modeled by a parabolic PDE system

4.1. Reactor description

We consider a tubular reactor, where an exothermic, irreversible second-order reaction of the form $A \rightarrow B$ takes place (Fig. 2). A cooling jacket of constant temperature is used to remove heat from the

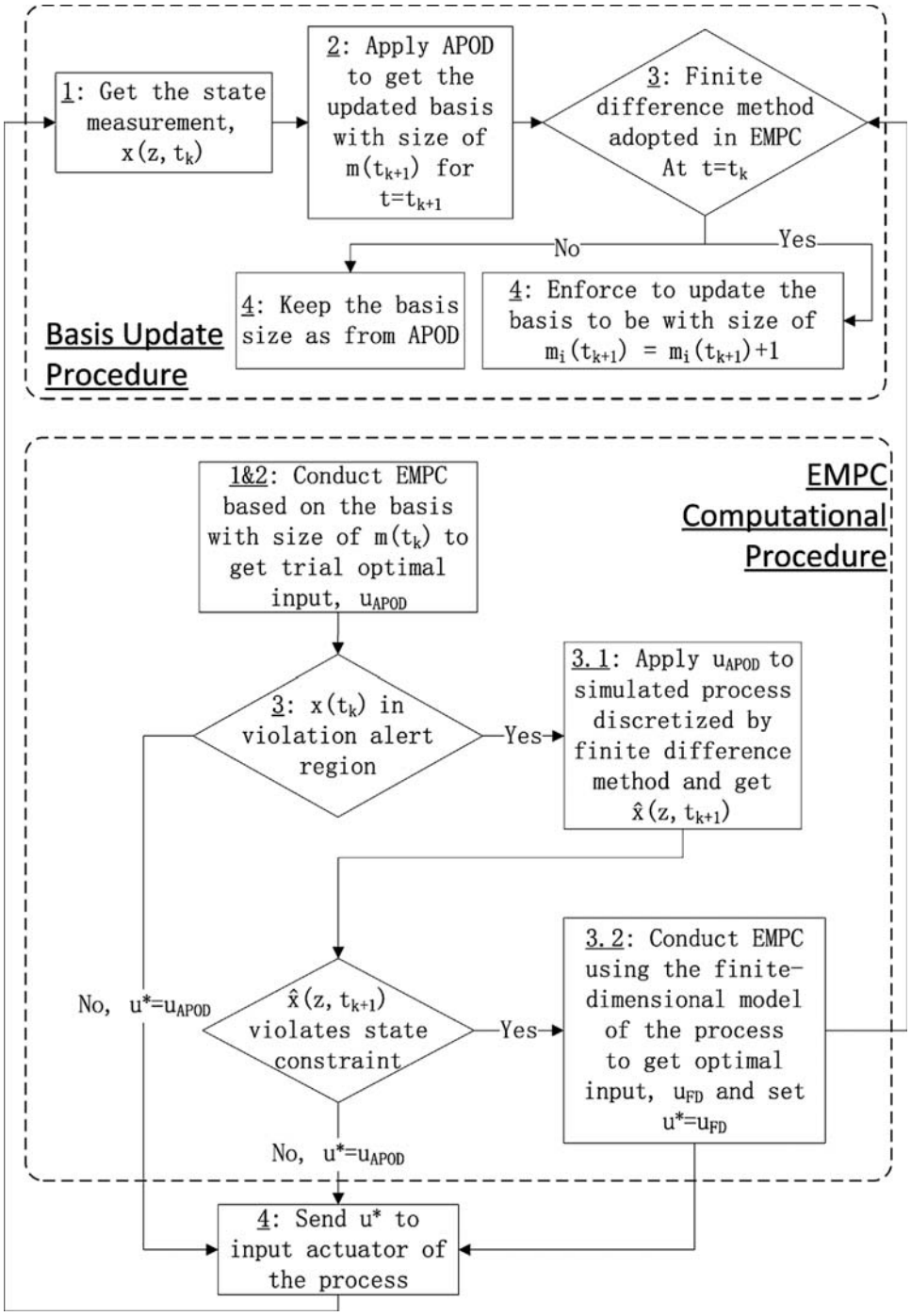

Fig. 1. EMPC system flow chart which integrates the APOD methodology with a finite-difference method to increase the computational efficiency and avoid potential state constraint violation.

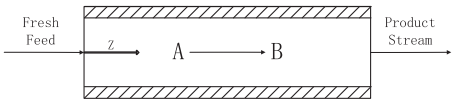

Fig. 2. A tubular reactor with reaction $A \rightarrow B$.

reactor. The states of the tubular reactor are temperature and concentration of reactant species A in the reactor, and the input is the inlet concentration of the reactant species A. In order to simplify the presentation of our results below, we use dimensionless variables and obtain the following nonlinear parabolic PDE model for the process (details and model notation can be found in [16] and [21]):

$$\begin{aligned}\frac{\partial x_1}{\partial t} &= -\frac{\partial x_1}{\partial z} + \frac{1}{Pe_1}\frac{\partial^2 x_1}{\partial z^2} + \beta_T(T_s - x_1) \\ &\quad + B_T B_C \exp\left(\frac{\gamma x_1}{1+x_1}\right)(1+x_2)^2 + \delta(z-0)T_i \\ \frac{\partial x_2}{\partial t} &= -\frac{\partial x_2}{\partial z} + \frac{1}{Pe_2}\frac{\partial^2 x_2}{\partial z^2} - B_C \exp\left(\frac{\gamma x_1}{1+x_1}\right)(1+x_2)^2 \\ &\quad + \delta(z-0)u\end{aligned} \tag{9}$$

where δ is the standard Dirac function, subject to the following boundary conditions:

$$\begin{aligned} z=0 \quad &: \quad \frac{\partial x_1}{\partial z} = Pe_1 x_1, \quad \frac{\partial x_2}{\partial z} = Pe_2 x_2; \\ z=1 \quad &: \quad \frac{\partial x_1}{\partial z} = 0, \quad \frac{\partial x_2}{\partial z} = 0; \end{aligned} \tag{10}$$

The following typical values are given to the process parameters: $Pe_1 = 7$, $Pe_2 = 7$, $B_T = 2.5$, $B_C = 0.1$, $\beta_T = 2$, $T_s = 0$, $T_i = 0$ and $\gamma = 10$. The following simulations were carried out using Java programming language in a Intel Core i7-2600, 3.40 GHz computer with a 64-bit Windows 7 Professional operating system.

4.2. Implementation of EMPC with adaptive proper orthogonal decomposition

We formulate an EMPC system like that of Eq. (7) for the tubular reactor with the ROM derived from the procedure described above. Ipopt [27] was used to solve the EMPC optimization problem. To numerically integrate the ODE model, explicit Euler's method was used with an integration step of 1×10^{-5} (dimensionless). Central finite-difference method was adopted to discretize, in space, the two parabolic PDEs and obtain a set of 101 ODEs in time for each PDE state (further increase on the order of discretization led to identical open-loop and closed-loop simulation results); this discretized model was also used to describe the process dynamics. In the first case studies reported below, with respect to EMPC settings, we used a prediction horizon, $N = 3$ and sampling time length, $\Delta = 0.01$ (dimensionless) which can sufficiently capture the appearance of new patterns by the newly available snapshots as the process moves through different regions in the state-space.

The cost function of Eq. (7) considered involves maximizing the overall reaction rate along the length of the reactor in the prediction horizon, t_k to t_{k+N} and over one operation period with $t_f = 1$. The temporal economic cost along the length of the reactor then takes the form:

$$L_e(t) = \int_0^1 r(z,t)dz \tag{11}$$

where $r(x_1(z,t), x_2(z,t)) = B_C \exp((\gamma x_1(z,t))/(1 + x_1(z,t)))(1 + x_2(z,t))^2$ is the reaction rate (dimensionless) in the tubular reactor.

The control input is subject to constraints as follows: $-1 \le u \le 1$. Owing to practical considerations, the amount of reactant material which can be fed to the tubular reactor over the period t_f is fixed. Specifically, $u(t)$ satisfies the following constraint over the period:

$$\frac{1}{t_f}\int_0^{t_f} u(\tau)d\tau = 0.5 \tag{12}$$

which will be referred to as the reactant material constraint. Details on the implementation of this constraint can by found in [16] and [15]. Furthermore, the temperature (dimensionless) along the length of the reactor is subject to the following constraint:

$$x_{1,\min} \le \min(x_1(z,t)), \quad \max(x_1(z,t)) \le x_{1,\max} \tag{13}$$

where $x_{1,\min} = -1$ and $x_{1,\max} = 3$ are the lower and upper limits, respectively.

To design the Lyapunov-based EMPC, a quadratic Lyapunov function of the following form was adopted for the constraint of Eq. (7g):

$$V(a_s(t)) = a_s^T(t) P a_s(t) \tag{14}$$

where P is an identity matrix of approximate dimension and $\overline{\rho} = 3$ (see [11] for more details on Lyapunov-based EMPC).

4.3. Simulation study

4.3.1. Case 1: APOD Compared to POD

This case study is introduced to demonstrate the effectiveness of the APOD method to capture process dynamic information (i.e., more accurate reduced order model) when compared with the traditional POD method; this comparison is conducted under the assumption that both APOD and POD methods are applied to a large snapshot ensemble.

To compute the empirical eigenfunctions, we use the set of 101 ODEs of each PDE in Eq. (9) (i.e., 101 discretized points). In detail, 15 different initial conditions and arbitrary (constant) input values, $u(t)$ were applied to the process model to get the spatiotemporal solution profiles with a time length of 2 (dimensionless). Consequently, from each simulation solution profile, 200 uniformly sampled snapshots were taken and combined to generate an ensemble of 3000 solutions which is noted as Ensemble 1. The POD method was applied to the developed ensemble of solutions to compute empirical eigenfunctions that describe the dominant spatial solution patterns embedded in the ensemble where the Jacobian in the POD method is calculated through a central finite-difference method. After truncating the eigenfunctions with relatively small eigenvalues ($\lambda_{ij} < \lambda_{min} = 1 \times 10^{-5}$), we were left with the first 4 eigenvalues for each state which occupy more than 99.99% (i.e., $\eta = 99.99\%$) of the total energy included in the entire ensemble. These 4 eigenfunctions for each PDE state are utilized for the POD method and as the initial eigenfunctions for APOD method to construct the ROM. To demonstrate the ability of APOD to capture the dominant trends that appear during closed-loop process evolution as the process goes through different regions of the state-space, we use EMPC of Eq. (7) based on POD using Ensemble 1 and based on APOD using Ensemble 1 (as the starting ensemble) to the tubular reactor, respectively. For the POD method, we constructed 2 ROMs which use the first 3 and 4 dominant eigenfunctions of the previously constructed eigenfunctions, respectively, for the EMPC system of Eq. (7). The EMPC utilizing ROM with 4 eigenfunctions is denoted as EMPC based on POD 1 and the other is denoted as EMPC based on POD 2.

The maximum temperature (dimensionless) profiles of the tubular reactor under the EMPC systems of Eq. (7) based on POD 1, POD 2 and APOD using Ensemble 1 are shown in Fig. 4. Since the temperature directly influences the reaction rate (i.e., higher temperature leads to higher reaction rate), the optimal operating strategy is to operate the reactor at the maximum allowable temperature. From Fig. 4, the EMPC system based on POD 1 and APOD operate the tubular reactor with a maximum temperature less than the maximum allowable which is a consequence of the error associated with the ROM. However, the process under the EMPC system based on POD 2 violates the state constraint imposed on $x_1(z,t)$ due to fewer eigenfunctions used for constructing the ROM in the EMPC system of Eq. (7). On the other hand, since the APOD is able to more accurately compute the state profile owing to its continuously updated dominant eigenfunctions, the EMPC system formulated with the ROM using APOD eigenfunctions operates the reactor at a greater temperature than the other EMPC system as demonstrated by the magnified plot in Fig. 4.

The computed manipulated input profiles from the EMPC systems of Eq. (7) based on POD 1 and APOD using Ensemble 1, respectively, over one period are shown in Fig. 3. From Fig. 3, the EMPC system based on APOD computes a less smooth manipulated input profile than that of the EMPC system based on POD 1 due to its continuously updated dominant eigenfunctions so that new process dynamics information is included in the dominant eigenfunctions. These updated dominant eigenfunctions improved the ROM which may be different from the previous ones when compared with the dominant eigenfunctions POD 1 used which are kept

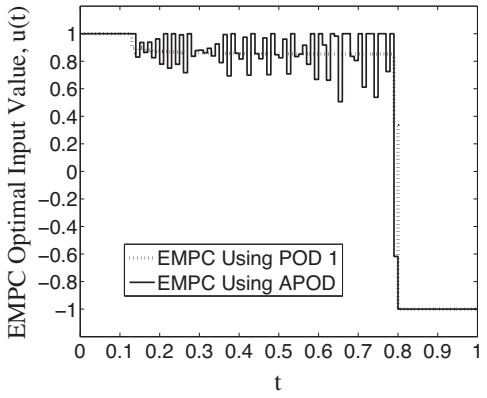

Fig. 3. Manipulated input profiles of the EMPC system of Eq. (7) based on POD 1 (dotted line) and APOD using Ensemble 1 (solid line) over one operation period.

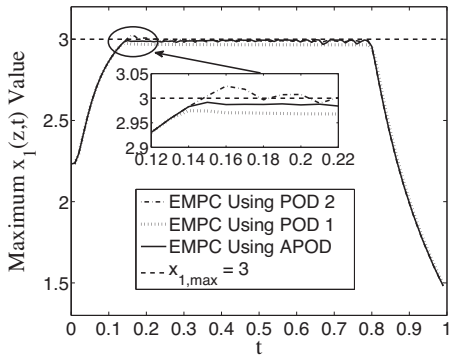

Fig. 4. Maximum $x_1(z, t)$ profiles of the process under the EMPC system of Eq. (7) based on POD 1 (dotted line), POD 2 (dash-dotted line)and APOD using Ensemble 1 (solid line) over one operation period.

the same during the whole operation period. Due to more accurate ROMs produced by APOD method, over one period $t_f = 1$, the total reaction rate of the process of Eq. (11) under the EMPC system based on APOD is 1.18% greater than that of the EMPC system based on POD 1.

Here, we have compared the EMPC calculation time for the EMPC systems of Eq. (7) based on POD 1 and APOD using Ensemble 1. As displayed in Fig. 5, the EMPC based on APOD achieves 38.8% improvement on the average computational time compared with that of the EMPC based on POD 1. As shown in Fig. 6, the APOD can adaptively adjust the required minimum number of eigenfunctions to satisfy the energy occupation requirement for each state while

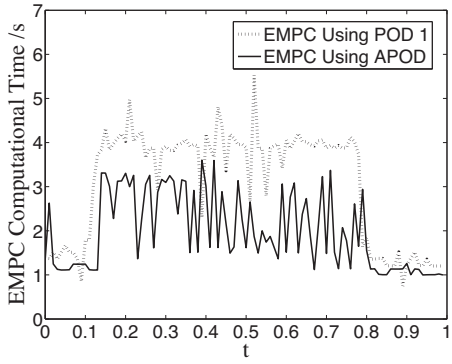

Fig. 5. EMPC computational time profiles for the EMPC system of Eq. (7) based on POD 1 (dotted line) and APOD using Ensemble 1 (solid line) over one operation period.

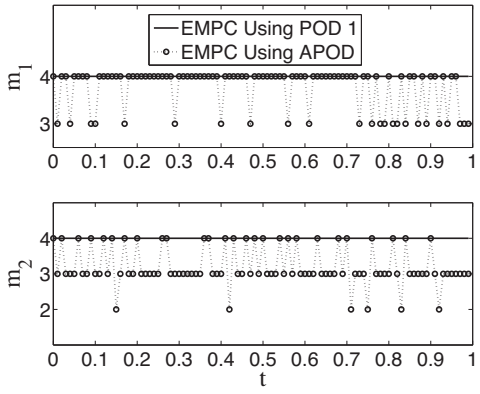

Fig. 6. Numbers of dominant eigenfunctions based on POD 1 (solid line) and APOD using Ensemble 2 (dotted line with circles) over one operation period.

the number of the eigenfunctions utilized by the POD 1 is fixed at $m_1 = m_2 = 4$. ROM using $m_1 = m_2 = 4$ of eigenfunctions increases the computational burden to the EMPC optimization problem based on POD 1 since the size of the dynamic model of Eq. (7b) is higher when compared with EMPC using APOD method. In terms of computational time of the recursive APOD procedure for updating basis eigenfunctions, it requires 45.2*s* on the average for the case of EMPC based on APOD using Ensemble 1. We note here that the APOD is completed before the EMPC problem is solved at $t = t_k$ ($k = 0, 1, \ldots$) which follows the methodology we proposed in Fig. 1. Therefore, for the EMPC calculation time in Fig. 5, the time of completing the APOD procedure is not included.

4.3.2. Case 2: APOD with an ensemble of small size

As we pointed out in Case 1, although the EMPC system based on APOD scheme using Ensemble 1 yields high state-approximation accuracy of the resulting ROM and of the process economic performance owing to the fact that the APOD continuously updates the dominant eigenfunctions, the APOD procedure and EMPC calculation is more computationally expensive when compared with that of the EMPC system based on a set of 101 ODEs for each PDE state. The computational efficiency difference is mainly caused by the number of the eigenfunctions adopted for constructing the ROM of the PDE system. Below, we construct the EMPC scheme using the APOD method with a small snapshot ensemble and demonstrate its advantage on computational efficiency and ability to on-line capture dynamic process information.

Based on the above consideration, in this case, we reduce the size of the ensemble by adopting an ensemble of 125 snapshots denoted as Ensemble 2 and apply Ensemble 2 to the APOD procedure for EMPC system of Eq. (7). The required energy occupation is still the same ($\eta = 99.99\%$). Moreover, from the practical point of applying the APOD to the process, the APOD procedure is completed by using the full state profile at $t = t_{k-1}$ for the dominant eigenfunctions at $t = t_k$ as we show in Fig. 1 which means the APOD can be completed during the sampling time. In detail, as long as we update the APOD during the sampling time, using the state value at the previous sampling time, $x(t_{k-1})$, we can complete the APOD update and this computational time has no effect on the EMPC computational efficiency. The computed manipulated input profiles from the EMPC systems of Eq. (11) based on APOD using Ensemble 1 and APOD using Ensemble 2, respectively, over one period are compared in Fig. 7. From Fig. 7, the EMPC system based on APOD using Ensemble 2 computes a less smooth manipulated input profile than that of the EMPC system based on APOD using Ensemble 1 due to the fact that fewer snapshots are used to get the dominant eigenfunctions. In terms of the process economic cost of Eq. (11), over one period $t_f = 1$, the total reaction rate of the process under the EMPC

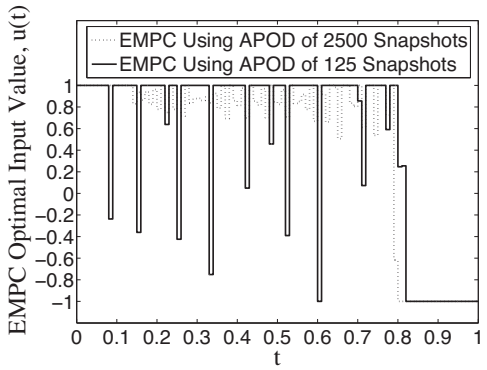

Fig. 7. Manipulated input profiles of the EMPC systems of Eq. (7) based on APOD using Ensemble 1 (dotted line) and on APOD (solid line) using Ensemble 2 over one operation period.

system based on APOD using Ensemble 2 is only 0.83% smaller than that of EMPC system based on APOD using Ensemble 1 and 1.74% smaller than that of the EMPC system based on the set of 101 ODEs for each PDE state.

We have compared the EMPC calculation time for the above EMPC systems based on APOD using Ensemble 1, APOD using Ensemble 2, and a model of a set of 101 ODEs for each PDE state in Fig. 8. As displayed in Fig. 8, the EMPC calculation time for the EMPC system based on APOD using Ensemble 2 is less than that of the EMPC system based on APOD using Ensemble 1. The computational time of EMPC system based on Ensemble 2 is 12.5% less than that of the EMPC system based on the model of a set of 101 ODEs for each PDE state. This computational efficiency improvement of the EMPC system based on APOD using Ensemble 2 results from the fact that fewer number of dominant eigenfunctions are adopted for constructing the ROM as compared in Fig. 9. We set a 99.99% energy occupation requirement for the APOD using Ensemble 1 and the corresponding number of eigenfunctions for each state is kept at $m_i = 4$, $i = 1, 2$ over one operation period; while for the EMPC based on the APOD using Ensemble 2, the corresponding number of eigenfunctions for each state adaptively changes as different process dynamics are collected and integrated into the dominant eigenfunctions. Moreover, the APOD using Ensemble 2 which has a much smaller size of ensemble also decreases the computational time of the APOD update procedure to 0.24*s*.

Since Ensemble 2 with a size of 125 snapshots only reflects part of process dynamics, it may not contain enough process dynamic behavior to guarantee the accuracy of the ROM of the PDE system.

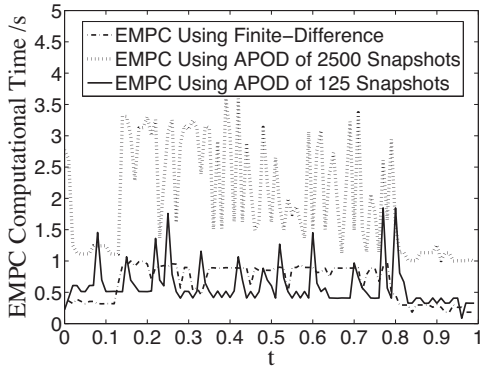

Fig. 8. EMPC calculation time profiles of the process under the EMPC systems of Eq. (7) based on APOD using Ensemble 1 (dotted line), on APOD using Ensemble 2 (solid line), and a set of 101 ODEs for each PDE state (dash-dotted line) over one operation period.

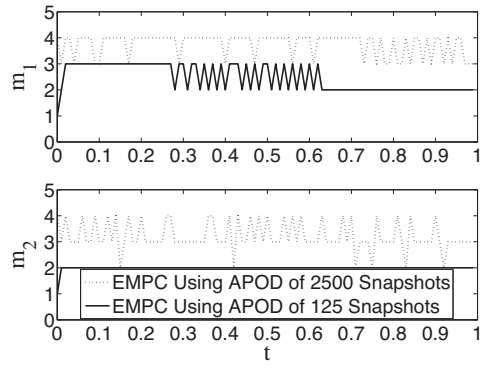

Fig. 9. Number of dominant eigenfunctions based on APOD using Ensemble 1 (dotted line) and on APOD using Ensemble 2 (solid line) over one operation period.

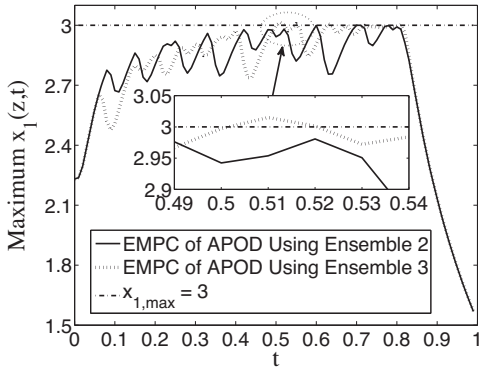

Fig. 10. Maximum x_1 profiles of the process under the EMPC systems of Eq. (7) based on APOD using Ensemble 2 (solid line) and on APOD using Ensemble 3 (dotted line) over one operation period.

Especially, when there exists a specific state constraint, the ROM may not be a good approximation of the original PDE system to help the EMPC avoid the state constraint violation due to its poor or incomplete state representation. In other words, the ROM either from POD or APOD may overestimate or underestimate the state value of Eq. (7b) in the EMPC optimization problem of Eq. (7). For the state constraint in this case, when the ROM underestimates the state value of $\max_z(\hat{x}_1(z,t))$, it may mislead the EMPC to compute and implement a higher optimal input value to the actual process which may result in the state constraint violation due to the second-order exothermic reaction rate. Here, we constructed another ensemble of 125 snapshots from different process solutions which is noted as Ensemble 3. We constructed EMPC systems using both of these 2 ensembles and applied them to the process. The maximum temperature (dimensionless) profiles of the tubular reactor under the EMPC systems of Eq. (7) based on APOD using Ensemble 2 and APOD using Ensemble 3 are shown in Fig. 10. From Fig. 10, the EMPC system based on APOD using Ensemble 2 operates the process around the maximum allowable temperature but at some points, it is close to the state constraint. While, from the magnified plot of Fig. 10, the EMPC system based on APOD using Ensemble 3 violates the state constraint around $t = 0.51$.

Remark 5. The number of snapshots affects not only the computational burden but also the state constraint satisfaction. A large size of ensemble usually results in more dominant eigenfunctions and at the same time, it increases the EMPC and APOD computational time. However, more eigenfunctions can improve the ROM accuracy and help the EMPC system to avoid the state constraint violation. Therefore, the choice of the number of snapshots (i.e., the

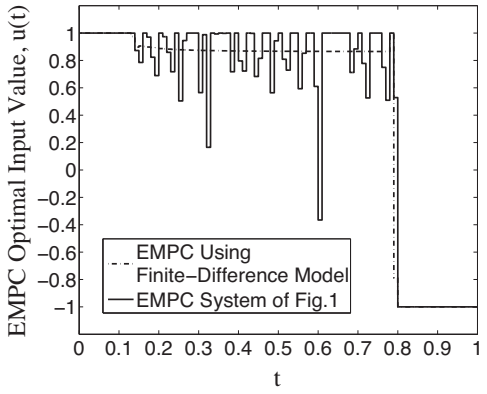

Fig. 11. Manipulated input profiles of the EMPC system of Fig. 1 (solid line) and the EMPC system of Eq. (7) based on the finite-difference method (dash-dotted line) over one operation period.

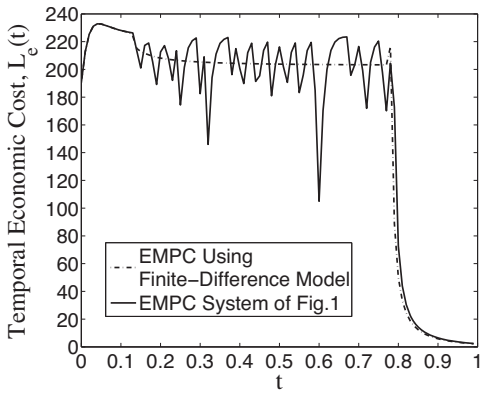

Fig. 12. Temporal economic cost along the length of the reactor, $L_e(t)$, of the EMPC system of Fig. 1 (solid line) and the EMPC system of Eq. (7) based on the finite-difference method (dash-dotted line) over one operation period.

number of the dominant eigenfunctions) is a tradeoff between the computational efficiency and reduced order model accuracy.

1 For POD method, the ensemble must have enough snapshots which contain as much global process dynamics as possible to help the EMPC system predict the state value more accurately. Since POD is only conducted once, it has no effect on the EMPC computational burden which only depends on how many modes/energy occupation is required.
2 For APOD method, the number of snapshots depends on the model accuracy although the ROM can be updated during the closed-loop operation. More snapshots will increase the APOD computational burden. But it will help the system avoid the state constraint violation. As long as the APOD update time is less than the sampling time size, we can use as many snapshots as possible, but large number of snapshots usually decreases the computational efficiency of the EMPC system.

4.3.3. Case 3: proposed flow chart of integrating APOD with finite-difference method

Based on the weakness of APOD with a small snapshot ensemble in state estimation accuracy which is shown by Case 2, in this case study, the proposed method of integrating APOD and finite differences is applied to construct the predictive models in EMPC scheme to achieve both computational efficiency and high reduced-order model accuracy (i.e., state estimation accuracy) so that the state constraint violation can be successfully avoided.

A set of 101 ODEs for each PDE state as the result of applying central finite-difference method to each PDE state is integrated into the EMPC scheme. An ensemble of 150 snapshots which is noted as Ensemble 4 is initially adopted for the EMPC system based on APOD method. We still request that the dominant eigenfunctions occupy $\eta = 99.99\%$ of the total energy of the ensemble. The EMPC system of Eq. (7) based on the finite-difference method resulting in a set of 101 ODEs for each PDE state is taken as the comparison method for the proposed EMPC formulation. The same prediction horizon, sampling time and integration step are adopted as the previous cases. We assume the state violation alert region, Ω_1, for dimensionless temperature, $x_1(z, t)$, is defined as:

$$\Omega_1 := \{x \in \mathbb{R} || \max(x_1(z, t_k)) - x_{1,\max}| \leq 0.05\} \quad (15)$$

The computed manipulated input profiles over one period $t_f = 1.0$ from the EMPC system of Fig. 1 and the EMPC system of Eq. (7) based on the finite-difference method over one period are shown in Fig. 11. From Fig. 11, the EMPC system of Eq. (7) based on the finite-difference method computes a smoother manipulated input profile than that of the EMPC of Fig. 1. The temporal economic cost profiles of the process under the EMPC of Fig. 1 and the EMPC system of Eq. (7) based on the finite-difference method are shown in Fig. 12. From Fig. 12, over one period $t_f = 1$, the total reaction rate of the process under the EMPC of Fig. 1 is only 0.33% smaller than that of the EMPC system of Eq. (7) based on the finite-difference model.

With respect to the performance of the EMPC, we have compared the maximum temperature (dimensionless) profiles of the tubular reactor under the EMPC systems as shown in Fig. 13. From Fig. 13, we see that the EMPC system of Fig. 1 can operate the process at the maximum allowable temperature and meanwhile avoid the state constraint violation issues by adopting the integrated EMPC system based on the finite-difference method when the process state value enters into the alert region of Eq. (15).

We finally have compared the calculation time of the EMPC system of Fig. 1 and the EMPC system of Eq. (7) based on the finite-difference method in Fig. 14. As displayed in Fig. 14, the EMPC of Fig. 1 achieves 8.71% improvement compared with the EMPC system of Eq. (7) based on the finite-difference method. In terms of Fig. 14, we point out that when the state value enters in the violation alert region, both the EMPC based on APOD method (to get a trial optimal input value) and the EMPC system of Eq. (7) based on the finite-difference method (to get an accurate optimal input value to help the EMPC scheme to avoid the state constraint violation if the previous optimal input value leads to constraint violation) are conducted which results in a longer computational time.

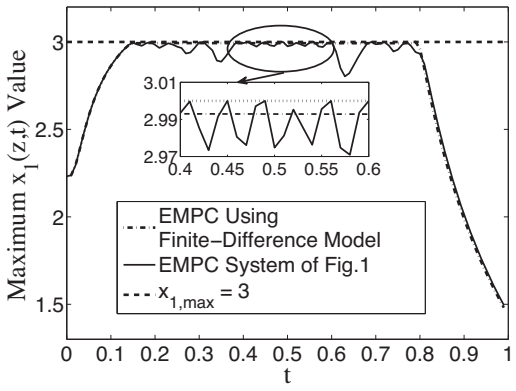

Fig. 13. Maximum $x_1(z, t)$ profiles under the EMPC system of Fig. 1 (solid line) and the EMPC system of Eq. (7) based on the finite-difference method (dash-dotted line) over one operation period.

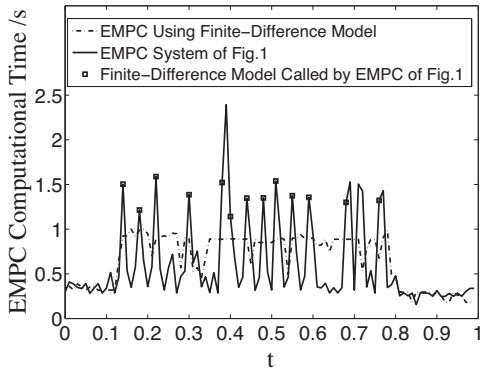

Fig. 14. EMPC computational time profiles for the EMPC system of Fig. 1 (solid line) and the EMPC system of Eq. (7) based on the finite-difference method (dash-dotted line) over one operation period.

Based on the above results and analysis, the proposed EMPC scheme of Fig. 1 successfully improves the whole computational efficiency while avoiding the state constraint violation.

Remark 6. We note here that the proposed EMPC scheme of Fig. 1 also has its drawbacks and limitations as follows:

1 Due to the automatic transition of the proposed EMPC scheme between APOD and finite-difference method after the process enters into the state violation alert region, the smoothness of the manipulated input trajectories is usually not guaranteed which may increase fluctuations on process state and economic-index trajectories in practice (e.g., production rate). This also reflects APOD method's limitation on capturing the global process dynamics and application on dynamic operation because of its requirement for a relatively smaller size of ensemble.
2 The proposed EMPC scheme achieves better computational efficiency compared with EMPC based on finite-difference method. If real-time computational constraints are not critical, EMPC based on a high-order finite-difference method which has a higher model accuracy would be a better choice. In terms of the limitation of the finite-difference method, if the size of the discretized model is large, EMPC based on this discretized model requires much more computational time compared with EMPC based on APOD method.

Remark 7. To deal with potentially large fluctuations of the optimal input profile brought by the proposed EMPC scheme of Fig. 1, an increase of the prediction horizon and an addition of an input fluctuation penalty term in the economic cost function of Eq. (11) may be adopted; such modifications of the presented EMPC scheme have been carried out and have demonstrated the expected benefit in reducing input fluctuations but are omitted here due to space limitations. It is important to note that a longer prediction horizon will definitely sacrifice the computational efficiency of EMPC and an input fluctuation penalty cost may also lead to a degradation of the process economic performance.

5. Conclusion

This work focused on developing an EMPC design for a parabolic PDE system which integrated the APOD method and a high-order finite-difference method to deal with control system computational efficiency and state constraint satisfaction. EMPC systems adopting POD, APOD, a high-order spatial discretization by central finite-difference method and the proposed EMPC flow chart were applied to a non-isothermal tubular reactor where a second-order chemical reaction takes place. These EMPC systems were compared with respect to their model accuracy, computational time, APOD update requirements, state constraint satisfaction and closed-loop economic performance of the tubular reactor. The simulation results demonstrated the advantages of APOD on improving computational efficiency of EMPC design, but also demonstrated a potential problem on state constraint violation. To address this issue, an EMPC scheme inheriting the high computational efficiency from APOD and the high state prediction accuracy from high-order finite-difference method is proposed; simulation results demonstrated that this EMPC scheme successfully improves the computational efficiency, while avoiding state constraint violations. Future work will focus on developing an output feedback EMPC scheme based on APOD in which the state measurements will be limited to few discrete points along the spatial domain.

Acknowledgements

Financial support from the National Science Foundation and the Department of Energy is gratefully acknowledged.

References

[1] R. Amrit, J.B. Rawlings, D. Angeli, Economic optimization using model predictive control with a terminal cost, Annu. Rev. Control 35 (2011) 178–186.
[2] D. Angeli, R. Amrit, J.B. Rawlings, On average performance and stability of economic model predictive control, IEEE Trans. Autom. Control 57 (2012) 1615–1626.
[3] A. Armaou, P.D. Christofides, Dynamic optimization of dissipative PDE systems using nonlinear order reduction, Chem. Eng. Sci. 57 (2002) 5083–5114.
[4] J.A. Atwell, B.B. King, Proper orthogonal decomposition for reduced basis feedback controllers for parabolic equations, Math. Comput. Model. 33 (2001) 1–19.
[5] S. Banerjee, J.V. Cole, K.F. Jensen, Nonlinear model reduction strategies for rapid thermal processing systems, IEEE Trans. Semicond. Manuf. 11 (1998) 266–275.
[6] P.D. Christofides, Nonlinear and Robust Control of PDE Systems: Methods and Applications to Transport-Reaction Processes, Birkhäuser, Boston, 2001.
[7] P.D. Christofides, P. Daoutidis, Finite-dimensional control of parabolic PDE systems using approximate inertial manifolds, J. Math. Anal. Appl. 216 (1997) 398–420.
[8] M. Ellis, H. Durand, P.D. Christofides, A tutorial review of economic model predictive control methods, J. Process Control 24 (2014) 1156–1178.
[9] B.A. Finlayson, The Method of Weighted Residuals and Variational Principles, Academic Press, New York, 1972.
[10] C. Foias, M.S. Jolly, I.G. Kevrekidis, G.R. Sell, E.S. Titi, On the computation of inertial manifolds, Phys. Lett. A 131 (1988) 433–436.
[11] M. Heidarinejad, J. Liu, P.D. Christofides, Economic model predictive control of nonlinear process systems using Lyapunov techniques, AIChE J. 58 (2012) 855–870.
[12] P. Holmes, J.L. Lumley, G. Berkooz, Turbulence, Coherent Structures, Dynamical Systems and Symmetry Cambridge University Press, New York, NY, 1996.
[13] R. Huang, L.T. Biegler, E. Harinath, Robust stability of economically oriented infinite horizon NMPC that include cyclic processes, J. Process Control 22 (2012) 51–59.
[14] R. Huang, E. Harinath, L.T. Biegler, Lyapunov stability of economically oriented NMPC for cyclic processes, J. Process Control 21 (2011) 501–509.
[15] L. Lao, M. Ellis, P.D. Christofides, Economic model predictive control of parabolic PDE systems: addressing state estimation and computational efficiency, J. Process Control 24 (2014) 448–462.
[16] L. Lao, M. Ellis, P.D. Christofides, Economic model predictive control of transport-reaction processes, Ind. Eng. Chem. Res. 53 (2014) 7382–7396.
[17] B. Luo, H. Wu, Approximate optimal control design for nonlinear one-dimensional parabolic PDE systems using empirical eigenfunctions and neural network, IEEE Trans. Syst. Man Cybern.: Part B 42 (2012) 1538–1549.
[18] S. Pitchaiah, A. Armaou, Output feedback control of dissipative PDE systems with partial sensor information based on adaptive model reduction, AIChE J. 59 (2013) 747–760.
[19] D.B. Pourkargar, A. Armaou, Modification to adaptive model reduction for regulation of distributed parameter systems with fast transients, AIChE J. 59 (2013) 4595–4611.
[20] S.S. Ravindran, Adaptive reduced-order controllers for a thermal flow system using proper orthogonal decomposition, SIAM J. Sci. Comput. 23 (2002) 1924–1942.
[21] W.H. Ray, Advanced Process Control, McGraw-Hill, New York, 1981.
[22] M.A. Singer, W.H. Green, Using adaptive proper orthogonal decomposition to solve the reaction-diffusion equation, Appl. Numer. Math. 59 (2009) 272–279.
[23] L. Sirovich, Turbulence and the dynamics of coherent structures. I – Coherent structures. II – Symmetries and transformations. III - Dynamics and scaling, Q. Appl. Math. 45 (1987) 561–590.

[24] J. Smoller, Shock Waves and Reaction-Diffusion Equations, Springer Verlag, Berlin, 1983.
[25] A. Theodoropoulou, R.A. Adomaitis, E. Zafiriou, Model reduction for optimization of rapid thermal chemical vapor deposition systems, IEEE Trans. Semicond. Manuf. 11 (1998) 85–98.
[26] A. Varshney, S. Pitchaiah, A. Armaou, Feedback control of dissipative PDE systems using adaptive model reduction, AIChE J. 55 (2009) 906–918.
[27] A. Wächter, L.T. Biegler, On the implementation of an interior-point filter line-search algorithm for large-scale nonlinear programming, Math. Program. 106 (2006) 25–57.